

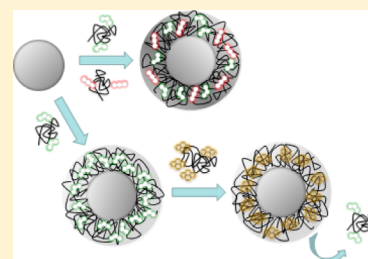
Polymer-Coated Nanoparticles by Adsorption of Hydrophobically Modified Poly(*N,N*-dimethylacrylamide)

Gema Marcelo,* J. M. G. Martinho, and José Paulo S. Farinha*

Centro de Química-Física Molecular and IN-Institute for Nanoscience and Nanotechnology, Instituto Superior Técnico, Av. Rovisco Pais, 1049-001 Lisboa, Portugal

Supporting Information

ABSTRACT: We prepared a reactive random copolymer of *N*-acryloxysuccinimide and *N,N*-dimethylacrylamide (DMA) by reversible addition–fragmentation chain transfer polymerization, with $M_n \approx 50k$ and 23 mol % reactive NAS groups. This copolymer was subsequently modified with hydrophobic (dodecyl) and fluorescent (pyrene, PY; phenanthrene, PHE; or anthracene, AN) side groups, to obtain fluorescent amphiphilic polymers with the same backbone and different substituents. These polymers were adsorbed onto model (ca. 130 nm diameter) poly(butyl methacrylate) nanoparticles, and the size and structure of the adsorbed layer were evaluated using a combination of fluorescence techniques and light scattering. The total diameter increases very fast with polymer concentration up to ca. 140 nm, and then more slowly to 154 nm, stabilizing at this value which corresponds to a polymer shell thickness of ca. 12 nm. In order to evaluate the distribution of hydrophobic groups on the adsorbed polymer layer, we used Förster resonance energy transfer between PHE- and AN-labeled poly(DMA) chains. The obtained concentration profile of the adsorbed polymer corresponds to a coated particle radius which is only slightly smaller than the hydrodynamic radius measured in the same conditions, indicating that the dyes are not located at the particle interface but mostly distributed across the adsorbed layer. Finally, we observed that hydrophobically modified PHE-labeled poly(DMA) chains adsorbed to the nanoparticles were very efficiently displaced by identical hydrophobically modified chains with five times their molecular weight ($M_n \approx 250k$) but labeled with PY.



INTRODUCTION

The synthesis, characterization, and structure–property relationships of polymer–colloid nanocomposites are currently of great interest to both academic and industrial scientists. Polymer adsorption onto the colloidal interface has been extensively studied¹ because by adding water-soluble polymers to colloidal suspensions one can control their interactions, which in turn affect phase behavior, rheological properties, etc.² Polymers are widely used as flocculants³ for suspensions in many industrial applications, such as mineral processing, paper-making, water treatment, and biotechnology. The effect of polymers on the stability of colloidal dispersions depends mainly on the adsorption of the macromolecules to the particle surface and the structure of the adsorbed layers that are formed. Polymer segments can physically adsorb to surfaces by electrostatic interaction, hydrophobic interaction, or ion binding.⁴ It is well-known that polymers bound to colloid particles can either impart stability through a steric mechanism,⁵ preventing the close approach of the colloid particles, or they can induce aggregation,⁶ for example, by “bridging” two or more particles.⁷ This behavior is in part controlled by the amount of polymer adsorbed on the particle surface, which depends on several factors such as polymer molecular weight, hydrophobicity, adsorption energy, solvent quality, its concentration in the dispersion, and the presence of specific groups.

At high polymer concentrations, the chains adsorb in a random and sequential manner onto the colloid surface. The

first chains to adsorb can establish many polymer segment–surface contacts, adopting a flattened or loopy conformation. Those that arrive at latter stages of the adsorption process encounter a nearly saturated surface and so exhibit progressively fewer polymer segment–surface contacts, until the equilibrium thickness of the adsorbed layer is achieved. The structure of the equilibrium adsorbed layer depends on the molecular composition of the polymer, determining the degree of chain stretching and surface coverage, and on the radius of curvature of the surface.⁸ The result of this adsorption mechanism can be described by a hairy carpet model⁹ that has been confirmed experimentally.¹⁰ The adsorption mechanism might be somehow different in the case of amphiphilic copolymers containing a small amount of hydrophobic groups, also known as hydrophobically modified polymers. In this case one anticipates that the hydrophobic groups will act as privileged anchoring points on the nanoparticle surface, but also that these groups can establish interchain contacts contributing to form much larger adsorbed layers than in the case of the nonmodified polymers.

Hydrophobically modified polymers have many important technological applications as rheology modifiers in foods, cosmetics, paints, etc.¹¹ They self-assemble in water forming

Received: December 11, 2012

Revised: February 8, 2013

different types of aggregates and can also adsorb onto colloidal particles to form a polymeric outer shell.¹² The adsorption behavior of these polymers onto nanoparticles has been studied mainly by following the hydrodynamic thickness of the adsorbed layer,¹³ mostly by scattering techniques,¹⁴ such as dynamic light scattering (DLS), small-angle neutron scattering (SANS), and small-angle X-ray scattering (SAXS).¹⁵ Although there are some examples of the use of other techniques, such as NMR diffusion and relaxation time studies,¹⁶ fluorescence techniques have been much less used to study the adsorption of polymers on colloidal surfaces.¹⁷ Fluorescent techniques, especially Förster resonance energy transfer (FRET), offer an excellent approach to characterize nanodomains in polymer systems¹⁸ because the length scale of FRET, typically from a few nanometers to tens of nanometers, matches that of many characteristic domains featured in polymer systems, namely those created around colloidal particles upon adsorption of polymers. Furthermore, the extreme sensitivity of FRET to the distance between energy donor and acceptor dyes¹⁸ allows one to determine their spatial distribution and, by comparing the distribution of the dyes from FRET with the adsorbed layer thickness calculated from the light-scattering results, obtain important information on the structure of the adsorbed layer.

One possible approach is to introduce FRET acceptor dyes in the nanoparticles and adsorb a hydrophobically modified polymer chain where some of the hydrophobic groups are FRET donor dyes. By assuming that the distribution of the donor dyes mimics that of all the hydrophobic groups in the polymer chain, the distribution of the polymer hydrophobic groups lying closer to the particle surface can be determined. Alternatively, one can adsorb a mixture of hydrophobically modified polymer chains, where some are labeled with a FRET donor dye and the others with an acceptor dye, onto unlabeled nanoparticles. By comparing the distribution of the hydrophobic groups obtained from FRET with the width of adsorbed polymer layer obtained by DLS, one can obtain structural information on the adsorbed layer and thus evaluate the role of the hydrophobic groups on the formation of a thicker adsorbed layer than that of the hairy carpet model.

In order to use FRET in polymer systems, the polymers should be labeled with small amounts (typically less than 1 mol %) of a fluorescent energy donor dye and an acceptor dye. It is important to have a controlled amount of dyes per chain and that the polymers have the same composition and low size dispersity. One strategy to obtain chains with predetermined composition, architecture, and molecular weight is to use a living/controlled polymerization (CRP) technique such as RAFT (reversible addition–fragmentation chain transfer).^{19–21} RAFT is very efficient in the CRP of acrylamide monomers²² and can be used to copolymerize a hydrophilic monomer, such as dimethylacrylamide (DMA), with a reactive monomer such as *N*-acryloxysuccinimide (NAS), which is a very efficient activated ester derivative.²³ This yields a reactive random copolymer, poly(DMA-*co*-NAS), in which the NAS groups can subsequently be used to attach different side groups to the same poly(DMA) chain backbone, itself a nonionic water-soluble polymer known to be biocompatible.²⁴ This strategy can be used to obtain identical amphiphilic copolymers of DMA containing fluorescent and nonfluorescent hydrophobic side groups.²²

In this paper, we first describe the preparation of two reactive random copolymers of DMA and NAS, one by conventional radical polymerization with $M_n \approx 250k$ and 2 mol % of reactive

NAS units, and the other by RAFT, with $M_n \approx 50k$ and 23 mol % of NAS. These are subsequently modified to incorporate hydrophobic octadecyl and fluorescent side groups. The amphiphilic copolymers were then adsorbed onto model polymer nanoparticles (ca. 130 nm diameter). Using a combination of fluorescence and light-scattering techniques, we characterize the structure of the adsorbed layer, notably regarding the position of the hydrophobic groups, and the exchange of the adsorbed chains by adding similar amphiphilic copolymers with larger molecular weight, labeled with a different dye.

■ EXPERIMENTAL SECTION

Materials. *N,N*-Dimethylacrylamide (DMA, Aldrich, 99%) was distilled under reduced pressure (75 °C; 10 mmHg) to remove the inhibitor. The comonomer, *N*-acryloxysuccinimide (NAS), was synthesized as previously described.²⁵ 2,2'-Azobis(isobutyronitrile) (AIBN, Fluka, 98%) was purified by recrystallization from ethanol, and *tert*-butyl dithiobenzoate (tBDB) was synthesized according to a previously published procedure.²⁶ *N,N*-diisopropylethylamine (DIPEA, Aldrich, 99.5%), tetrahydrofuran (THF, Aldrich, 99%), *n*-hexane (LAB-SCAN, 95%), *tert*-butyl alcohol (Riedel-de-Haën, 99+%), and dimethylformamide (DMF, Aldrich, 99.8%) were dried (under sodium or CaH₂) and distilled before use. 1,4-Dioxane (Acros, 99%) was distilled over LiAlH₄ (110 °C). All the purified chemicals were stored in the dark, at low temperature and under positive pressure of nitrogen. Dodecylamine (Aldrich, 98%), dimethylamine (Aldrich, 99+%), sodium dodecyl sulfate (SDS, SIGMA, 99%), trioxane (Acros, 99%), diethyl ether (SDS, 99.5%), and dichloromethane (SDS, 99.9%) were used without further purification. Details about the synthesis of the fluorophores used in this work, [4-(1-pyrenyl)butyl]amine hydrochloride, [4-(9-anthracenyl)butyl]amine hydrochloride, [4-(9-phenanthrenyl)butyl]amine hydrochloride, and the monomer 4-(anthracene-2-yl)butyl methacrylate, are reported elsewhere.^{27,28} Coumarin 153 (C153, Fluka, 98%) and octadecylrhodamine B (Molecular Probes) were used as received.

For the nanoparticles preparation, butyl methacrylate (BMA, Aldrich) and ethylene glycol dimethacrylate (EGDMA, Aldrich) were distilled under vacuum prior to use. Potassium persulfate (KPS, Aldrich), sodium bicarbonate (NaHCO₃, Aldrich), dodecyl mercaptan (C₁₂SH, Aldrich), and sodium dodecyl sulfate (SDS, Aldrich) were used as received.

Polymer Synthesis. Two reactive random copolymers of *N,N*-dimethylacrylamide (DMA) and *N*-acryloxysuccinimide (NAS) were synthesized by radical polymerization using different techniques. The first DMA/NAS random copolymer, poly(DMA_{250k}-*co*-NAS), with $M_n \approx 250k$ and 2 mol % of reactive NAS units, was synthesized by conventional radical polymerization of DMA with NAS in *tert*-butyl alcohol, at 70 °C under nitrogen, using 2,2'-azobis(isobutyronitrile) as initiator.^{29,30} The lower molecular weight random copolymer, poly(DMA_{50k}-*co*-NAS), with $M_n \approx 50k$ and 23 mol % of NAS, was prepared by controlled radical polymerization using the reversible addition–fragmentation chain transfer (RAFT) technique.²² RAFT offers an excellent control of molecular weight and composition, with small molar mass dispersity.^{21,31} DMA and NAS were polymerized using 4,4'-azobis(isobutyronitrile) as initiator and *tert*-butyl dithiobenzoate as chain transfer agent (CTA). Details of this synthesis are

described elsewhere.^{22,30,32} The characteristics of the two copolymers are summarized in Table 1.

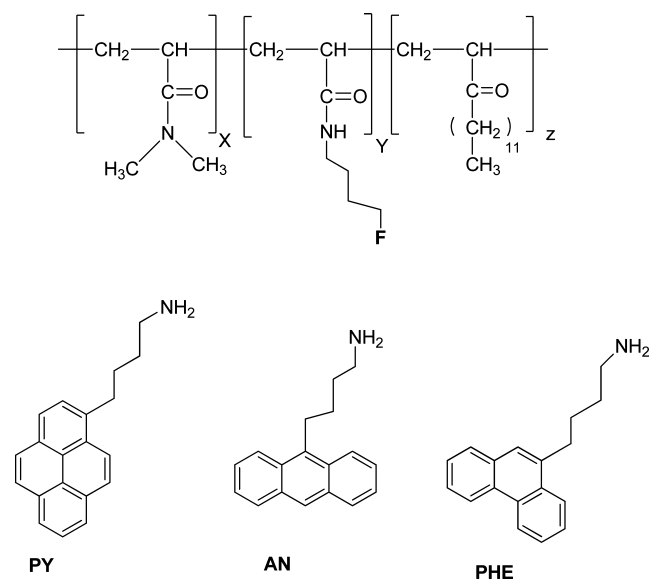
Table 1. Characteristics of the Reactive DMA/NAS Random Copolymers

	p(DMA _{250k} -co-NAS)	p(DMA _{50k} -co-NAS)
number average molecular weight (M_n) ^a	251 600 g·mol ⁻¹	49 200 g·mol ⁻¹
polydispersity index (M_w/M_n) ^a	2.20	1.21
molar composition ^b	DMA 98 mol % NAS 2 mol %	DMA 77 mol % NAS 23 mol %

^aDetermined by aqueous SEC/MALS. ^bDMA and NAS content determined by ¹H NMR.

Polymer Labeling. Samples of hydrophobically modified poly(*N,N*-dimethylacrylamide) were prepared by labeling the reactive copolymers precursors poly(DMA_{250k}-co-NAS) and poly(DMA_{50k}-co-NAS) with dodecylamine (DO) and the fluorophores shown in Scheme 1,³³ [4-(1-pyrenyl)butyl]amine hydrochloride (PY), [4-(9-anthracenyl)butyl]amine hydrochloride (AN), and [4-(9-phenanthrenyl)butyl]amine hydrochloride (PHE).²⁷

Scheme 1. Top: Chemical Structure of the Hydrophobically Modified Poly(DMA) Copolymers; F = PY, AN, or PHE. Bottom: Fluorescent Dyes Used in the Labeling Reaction of the Copolymer Precursors



The unreacted NAS units remaining after the polymer modification were removed by bubbling dimethylamine into the reaction mixture. This also allows us to convert the dithioester CTA at the chain end to a thiol group, thus surprising quenching of the dyes' fluorescence.³⁴

The final content of dyes incorporated in the labeled polymers was calculated by UV-vis absorption. The presence of the alkyl chain groups in the polymers decreases their solubility in methanol and leads to dye aggregation that influences the correct determination of label content. To avoid this problem the polymers were dissolved in 500 mM SDS aqueous dispersions, for which the surfactant concentration is well above its critical micelle concentration in pure water (8

mM).^{35,36} The molar extinction coefficients of the free dyes, PY ($\epsilon_{345\text{ nm}} = 37\,300\text{ dm}^3\text{ mol}^{-1}\text{ cm}^{-1}$), AN ($\epsilon_{351\text{ nm}} = 3\,680\text{ dm}^3\text{ mol}^{-1}\text{ cm}^{-1}$), and PHE ($\epsilon_{299\text{ nm}} = 10\,600\text{ dm}^3\text{ mol}^{-1}\text{ cm}^{-1}$) were also obtained in 500 mM SDS aqueous dispersions. The content in DO groups was determined by ¹H NMR in D₂O or CDCl₃, using a Bruker Avance 200 MHz spectrometer.³³ The characteristics of the hydrophobically modified polyDMA copolymers are summarized in Table 2.

Table 2. Copolymer Composition

copolymer	dye content ^a	dodecyl acrylamide content ^b
p(DMA _{250k} /PY ₁₂ /DO ₃₈)	0.47 mol % PY (ca. 12 PY groups/chain)	1.50 mol % (ca. 38 DO groups/chain)
p(DMA _{50k} /AN ₂ /DO ₁₈)	0.41 mol % AN (ca. 2 AN groups/chain)	3.74 mol % (ca. 18 DO groups/chain)
p(DMA _{50k} /PHE ₃ /DO ₁₀)	0.62 mol % PHE (ca. 3 PHE groups/chain)	1.96 mol % (ca. 10 DO groups/chain)

^aDetermined by UV-vis spectroscopy. ^bDetermined by ¹H NMR.

Polymer Nanoparticle Preparation. Polymer nanoparticle dispersions were prepared by seeded semicontinuous emulsion polymerization as previously described.³⁷ Cross-linked seed particles were prepared from a 4/3 molar ratio of BMA and EGDMA by batch emulsion polymerization at 80 °C under nitrogen in a three-necked glass reactor fitted with a condenser and a mechanical stirrer.³⁸ The monomers, surfactant, and NaHCO₃ were mixed with water. The mixture was stirred and degassed by nitrogen bubbling for 30 min and then heated to 80 °C. After addition of the initiator KPS solution, stirring continued for another 2–3 h under nitrogen, to obtain a 5 wt % dispersion of particles with a diameter of ca. 21 nm.

The seed particles were used to prepare the unlabeled polymer nanoparticles (PNP) in a 250 mL three-neck flask, equipped with a condenser and a mechanical stirrer. The dispersion was purged with N₂ for 30 min and then heated to 80 °C under nitrogen. A KPS aqueous solution and the mixture containing BMA, dodecyl mercaptan, and SDS were introduced into the reactor at a constant feed rate over 6 h. After complete addition, the reaction mixture was stirred and heated for another 2 h to produce a dispersion with ca. 20 wt % solids content with a particle diameter of (127 ± 4) nm.

For the preparation of the anthracene-labeled PBMA nanoparticles (PNP-AN), we used the same seed dispersion but changed the recipe of the particle shell by substituting 1 mol % of the monomer content by 4-(anthracene-2-yl)butyl methacrylate.²⁸ The final dispersion had ca. 19 wt % solids content and a particle diameter of (129 ± 6) nm.

Sample Preparation. Samples for DLS measurements were prepared by dissolving p(DMA_{50k}/PHE₃/DO₁₀) in THF and adding water dropwise into the THF solution. The final aqueous solution contains a 2 wt % in THF. Different aqueous solutions containing p(DMA_{50k}/PHE₃/DO₁₀) concentrations ranging from 4 × 10⁻⁸ to 1 × 10⁻³ g/mL were prepared. Finally, an aqueous dispersion of PNP was added to the polymer aqueous solutions (final PNP solid content of 0.019 wt %). The mixture was left shaking overnight before performing DLS measurements.

Mixtures of p(DMA_{50k}/PHE₃/DO₁₀) and p(DMA_{50k}/AN₂/DO₁₈) in water were prepared by mixing the stock solution of both polymers in THF and later adding water dropwise, with the final aqueous solution containing 2 wt % THF. Two

solutions of both polymers in water with molar ratios (Phe/An) ranging from 0 to 1, and total polymer concentrations 1.18×10^{-5} and 7.25×10^{-4} g/mL were prepared. After that, an aqueous dispersion of PNP was added in each polymer aqueous solution, up to a final PNP solid content of 0.019 wt %.

For the energy transfer measurements in the polymer shell coating the PNP, aqueous solutions of p(DMA_{50k}/PHE₃/DO₁₀) and p(DMA_{50k}/AN₂/DO₁₈) at a total concentration of polymer of 1.18×10^{-5} g mL⁻¹ were prepared and later were mixed with PNP as mentioned above for the DLS sample preparation.

Samples for energy transfer measurements between the phenanthrene labeled polymer shell and the anthracene in the PNP-AN core were prepared by mixing (and shaking overnight) aqueous solutions of p(DMA_{50k}/PHE₃/DO₁₀) in concentrations from 4×10^{-8} to 1×10^{-3} g/mL, with an aqueous dispersion of PNP-AN with a final particle solid content of 0.019 wt %.

For FCS measurements using octadecyl rhodamine B (ORB), a 1×10^{-6} M stock solution of ORB in EtOH was prepared. Sixteen microliters of this solution were added to 4 mL of a 0.019 wt % aqueous dispersion of PNP and homogenized overnight. Either p(DMA_{50k}/PHE₃/DO₁₀) (9.8×10^{-5} g/mL) or p(DMA_{250k}/PY₁₂/DO₃₈) (1.02×10^{-5} and 2.63×10^{-5} g/mL) was adsorbed onto the PNP containing the adsorbed ORB (same procedure as for the DLS sample preparation).

All mixtures of polymer and nanoparticles were left shaking overnight after preparation and then 4 h without stirring before each experiment.

Instrumentation. Dynamic light-scattering measurements were performed in a Brookhaven instrument (BI-200SM Goniometer and BI-9000AT correlator) using a He-Ne laser (632.8 nm, 35 mW, model 127, Spectra Physics) and an avalanche photodiode detector. The measurements were carried out in a glass cylindrical cell immersed in a circular vat cell containing decaline, in order to simplify the corrections needed for refractive index variations and minimize light refraction. The DLS data were analyzed using the CONTIN method (Brookhaven analysis package) and a cumulant expansion,³⁹ to determine the translational diffusion coefficient, from which the hydrodynamic radius (R_H) of the copolymer micelles is calculated by the Stokes–Einstein equation for noninteracting spheres:

$$R_H = \frac{kT}{6\pi\eta_0 D_0} \quad (1)$$

where k is the Boltzmann constant, T is the absolute temperature, η_0 is the solvent viscosity, and D_0 is the diffusion coefficient at infinite dilution.

Steady-state fluorescence measurements were carried out in a SPEX Fluorolog F112A spectrofluorimeter and a SLM-Aminco 8110 Series 2 spectrofluorometer. The UV–vis absorption spectra were measured in a Shimadzu UV-3101PC UV–vis–NIR spectrophotometer.

Fluorescence decay measurements with picosecond resolution were obtained by the single photon timing technique in a previously described setup.⁴⁰ The experimental fluorescence decay curves were analyzed using software that simulates parametrized model decay curves and uses a nonlinear least-squares reconvolution method based on the Marquard

algorithm to compare the simulated curves with the experimental decays.⁴¹

Fluorescence correlation spectroscopy (FCS) curves were obtained with a Leica TCS SP5 laser scanning microscope using a HCX-PL-PO-CS-1.20W 63× water immersion objective, using an ISS VISTA correlator and software. The correlation curves were analyzed with the 3D-Gaussian ratio model.

RESULTS AND DISCUSSION

Critical Aggregation Concentration of p(DMA_{50k}/PHE₃/DO₁₀). The critical aggregation concentration (CAC) for the p(DMA_{50k}/PHE₃/DO₁₀) copolymer in water was determined from both the variation in fluorescence intensity and wavelength of maximum emission of Coumarin 153 (C153) with polymer concentration. The solvatochromism of C153 reports the reorganization of its surroundings, due to the substantial increase of the dipole moment upon excitation.⁴² Aggregates can show various microenvironments throughout their structure: the micellar core is hydrophobic; the water-rich shell is hydrophilic; and the core–shell interface has an intermediate environment. Using C153, which has a low fluorescence quantum yield in hydrophilic environments and a high quantum yield in hydrophobic environments, we could determine the CAC of the copolymer in water. Samples of the copolymer p(DMA_{50k}/PHE₃/DO₁₀) with concentrations ranging from ca. 30 μg/L to 1.1 g/L and a constant C153 concentration [C153] \approx 0.45 μM were used to determine the CAC of the copolymer at 20 °C (Figure 1), from the increase in fluorescence intensity and the hypsochromic shift of the C153 fluorescence spectra as the p(DMA_{50k}/PHE₃/DO₁₀) concentration increases in water. At a given onset concentration, a pronounced increase in the fluorescence intensity and a large shift in the wavenumber of maximum emission, $\bar{\nu}_{\max}$ was observed due to the increasing partition of the dye from the aqueous medium to the hydrophobic aggregates. The CAC values obtained from the fluorescence intensity and the solvatochromic shift are 7.0×10^{-5} and 9.5×10^{-5} g/mL, respectively.

PBMA Nanoparticles. The hydrodynamic radii of the PBMA nanoparticles (PNP) were determined by DLS and fluorescence correlation spectroscopy (FCS). The hydrodynamic radius measured by DLS for the unlabeled PNP was (127 ± 4) nm and for the anthracene-labeled nanoparticles (PNP-AN) was (129 ± 6) nm. We also checked the hydrodynamic diameter of the particles by FCS, using octadecylrhodamine B (ORB), which was added to the nanoparticles in water dispersion (0.019 wt %). The spectroscopic behavior of ORB is similar to that of Rhodamine B, but it is more influenced by the formation of H and J dimers in aqueous media as a result of hydrophobically driven association. The fluorescence of ORB in water is strongly self-quenched by aggregate formation, a fact that is very important for the binding studies and interpretation of the FCS data: ORB dyes in water are practically nonfluorescent, and we are able to detect the ORB adsorbed into the nanoparticles without a significant influence of ORB molecules in water.⁴³ The FCS correlation curve of the PNP with adsorbed ORB at 25 °C was fitted with a model for two species, one with a diffusion coefficient of $280 \mu\text{m}^2/\text{s}$ (which corresponds to free ORB in water⁴³) and the other with a diffusion coefficient of $3.41 \mu\text{m}^2/\text{s}$, which corresponds to a hydrodynamic radius of

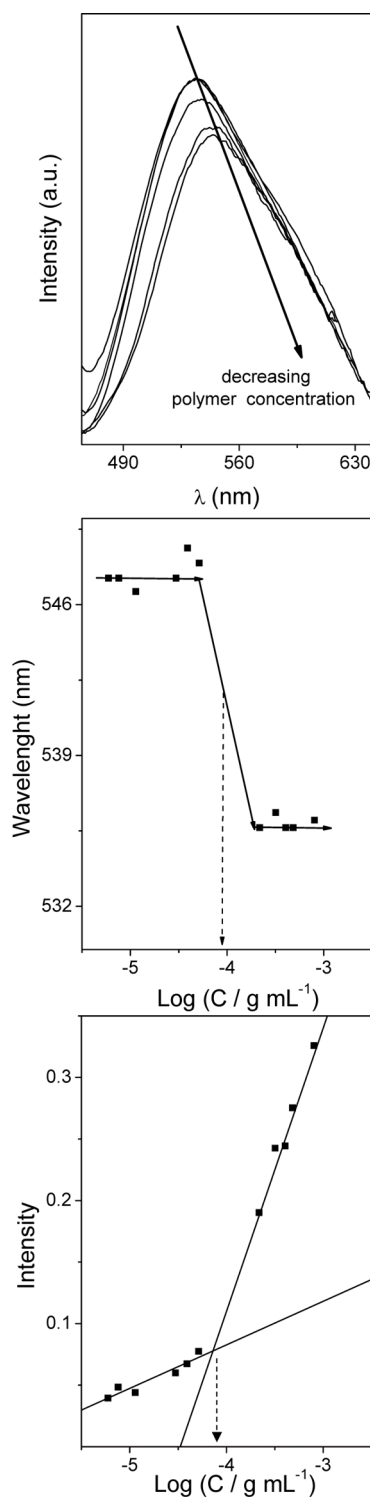


Figure 1. (A) C153 fluorescence spectra at different p(DMA_{50k}/PHE₃/DO₁₀) concentrations in water with 0.45 μ M C153 at 20 $^{\circ}$ C (excitation wavelength λ_{exc} = 410 nm). (B) Wavelength of maximum intensity, and (C) maximum fluorescence intensity, of the C153 spectrum as a function of p(DMA_{50k}/PHE₃/DO₁₀) concentration.

$R^{\text{FCS}} = 126$ nm, in good agreement with the value obtained by DLS (127 nm).

Hydrophobically Modified Copolymer. Dynamic light scattering of p(DMA_{50k}/PHE₃/DO₁₀) in water at 2.4×10^{-5} g/mL (below the CAC of the polymer) yielded the hydrodynamic diameter of the single chains in water, $D_h^{\text{UNI}} = 3.4$ nm (Figure

2A). For a concentration of 6×10^{-5} g/mL (at the polymer CAC), a narrow distribution of aggregates was obtained, with a

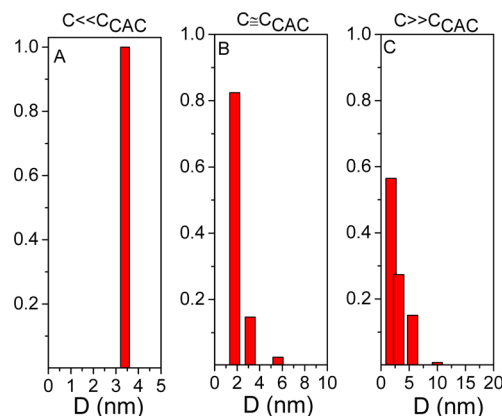


Figure 2. Number-averaged distribution of hydrodynamic diameter obtained by DLS as a function of p(DMA_{50k}/PHE₃/DO₁₀) concentration: (A) below the CAC, at 2.4×10^{-5} g/mL; (B) at the CAC, 6.0×10^{-5} g/mL; (C) above the CAC, at 2.0×10^{-4} g/mL.

number-weighted average radius of 3.7 nm (Figure 2B). By increasing the polymer concentration well above the CAC, for example at 2×10^{-4} g/mL, the distribution of aggregate changes, increasing the number-weighted average radius to 4.3 nm, which does not change with time over a week (Figure 2C).

Adsorption of p(DMA_{50k}/PHE₃/DO₁₀) onto the Polymer Nanoparticles. On adsorption studies, there have been two conventional ways to characterize the effects of adsorbed or grafted polymers on colloidal interactions. One is to gradually increase colloidal volume fraction while keeping the polymer coverage identical,^{44,45} the other, usually aimed at resolving the steric repulsion imparted by polymer, is to fix the colloidal volume fraction while gradually increasing the amount of polymer.⁴⁵ The latter approach was used in our study, with different concentrations of p(DMA_{50k}/PHE₃/DO₁₀) copolymer being adsorbed onto a fixed amount of PBMA nanoparticles (PNP). The hydrodynamic radii of copolymer-coated PNP were determined by DLS after addition of the copolymer and equilibration for 24 h (Figure 3A). Figure 4 shows the hydrodynamic diameter dependence on polymer concentration and the number-averaged diameter distributions at four concentrations. When the polymer concentration increases, the distribution of diameters is displaced to higher values as the adsorbed polymer shell thickness increases. The increase in particle size with polymer concentration, initially very steep, slows after the CAC to finally stabilize at a diameter value of ca. 154 nm. While below the CA the adsorbed shell increases by adsorption of isolated chains, above the CAC the mechanism probably involves adsorption of the aggregates, followed by (slower) rearrangement to a uniform shell. The size dispersity is relatively low and does not increase appreciably with the concentration of polymer approximately up to the CAC, indicating that for the adsorption of isolated chains, the distribution of the hydrophobically modified polymer on the nanoparticles is uniform. The adsorption of aggregates above the CAC results in an increased size dispersity, visible at 5.4×10^{-4} g/mL of polymer (Figure 4D).

In order to confirm the hydrodynamic diameter values obtained by DLS, the coated particles obtained by adsorption from a 9.8×10^{-5} g/mL polymer concentration (above the

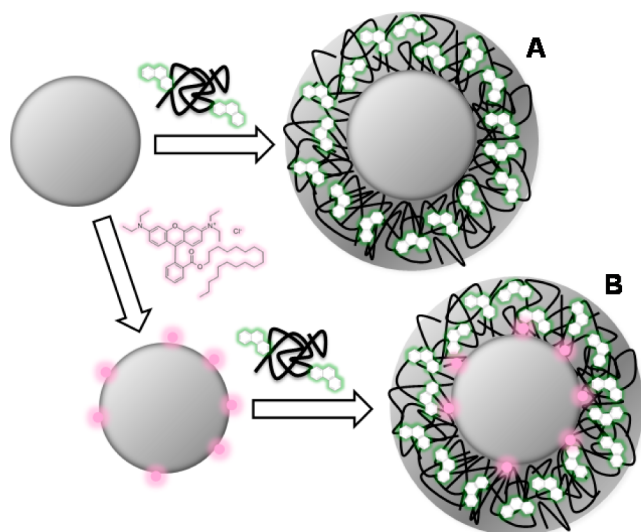


Figure 3. Hydrodynamic radii of copolymer-coated PNP were determined by DLS after addition of the copolymer and equilibration for 24 h (A). To perform FCS measurements, octadecylrhodamine B (ORB) was added to the PNP, which were subsequently coated with the hydrophobically modified copolymer (B).

polymer CAC, with an hydrodynamic diameter of 143.8 nm by DLS) were measured by FCS, on particles to which we adsorbed ORB before the adsorption of the copolymer (Figure 3B). The correlation curves have two diffusion coefficients, one of $280 \mu\text{m}^2/\text{s}$ (residual free ORB in water) and another of $2.97 \mu\text{m}^2/\text{s}$, corresponding to a hydrodynamic diameter of 144.8 nm, that coincides with the value obtained by DLS.

Conformation of the Adsorbed Polymer Shell by FRET. In order to characterize the conformation of the polymers in the adsorbed shell, we used Förster resonance energy transfer (FRET). We first adsorbed different amounts of phenanthrene-labeled copolymer, $\text{p(DMA}_{50\text{K}}/\text{PHE}_3/\text{DO}_{10})$, onto the anthracene-labeled PBMA nanoparticles (PNP-AN). FRET can then occur from the phenanthrene (donor) dyes in the copolymer to the anthracene (acceptor) dyes inside the particle (Figure 5A). In a second experiment, we adsorbed polymers with the same backbone but labeled with either donor or acceptor dyes, $\text{p(DMA}_{50\text{K}}/\text{PHE}_3/\text{DO}_{10})$ and $\text{p(DMA}_{50\text{K}}/\text{AN}_2/\text{DO}_{18})$, onto the unlabeled PNPs (Figure 5B). In this case, FRET occurs within the adsorbed polymer shell, and the analysis of the fluorescence decay curves allow the determination of the distribution of donor and acceptor dyes in the shell.¹⁸ Since the dyes are covalently attached to the polymer chains, we can obtain information on the conformation of the adsorbed copolymer.

In Figure 6A we show the emission spectra (with $\lambda_{\text{exc}} = 295 \text{ nm}$ excitation) for different concentrations of $\text{p(DMA}_{50\text{K}}/\text{PHE}_3/\text{DO}_{10})$ copolymer adsorbed onto PNP-AN (0.019 wt % in water). Although at this wavelength only phenanthrene is directly excited, the spectra shows the emission of both phenanthrene and anthracene (maximum intensity at wavelengths $\lambda_{\text{Phe}} = 350 \text{ nm}$ and $\lambda_{\text{Ant}} = 400 \text{ nm}$, respectively), because FRET occurs from phenanthrene to anthracene at the interface between the nanoparticle and the adsorbed polymer shell. In fact, for polymer concentrations below $7.5 \times 10^{-5} \text{ g/mL}$, only anthracene emission is observed because the adsorbed layer is thin enough that all the phenanthrene donor groups are in close proximity to the anthracene groups in the nanoparticle,

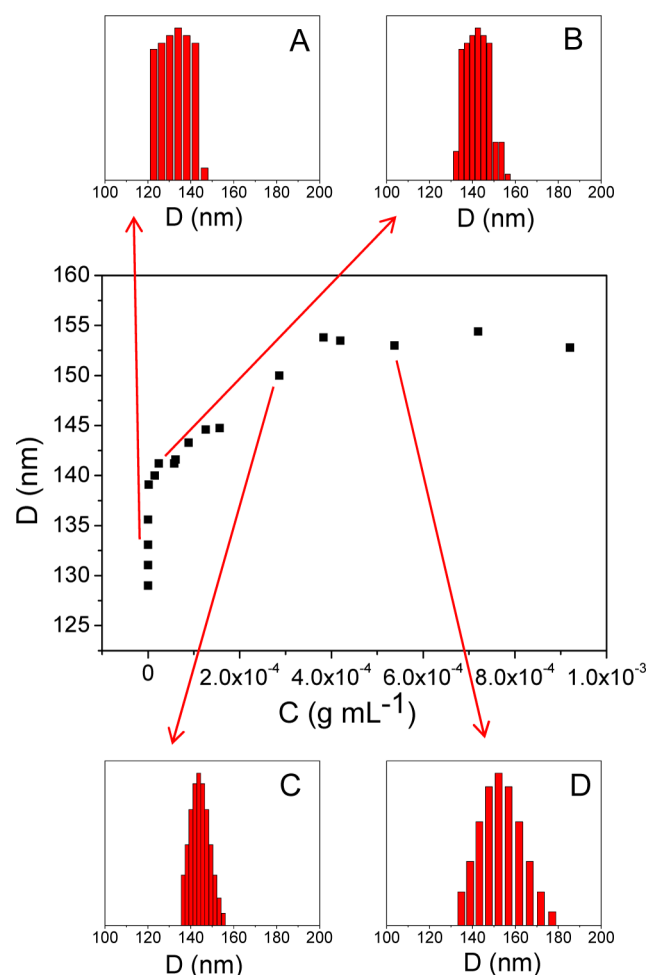


Figure 4. Hydrodynamic diameter of PNP-AN (at 0.019 wt %) with different concentrations of adsorbed $\text{p(DMA}_{50\text{K}}/\text{PHE}_3/\text{DO}_{10})$. The number-averaged diameter distributions at four polymer concentrations (A, $3.8 \times 10^{-7} \text{ g/mL}$; B, $2.3 \times 10^{-5} \text{ g/mL}$; C, $2.9 \times 10^{-4} \text{ g/mL}$; D, $5.4 \times 10^{-4} \text{ g/mL}$) show that the adsorption of the hydrophobically modified polymer on the nanoparticles originates coated nanoparticles of controllable diameter and low size dispersity up to the CAC of the polymer.

and consequently the efficiency of energy transfer is close to 100%.

Although the intensity of the spectra increases as the concentration of phenanthrene-labeled polymer increases (as expected), if we correct the phenanthrene emission with the amount of light absorbed by the phenanthrene dyes (Figure 6B), we can discriminate the effect of FRET. In the absence of energy transfer, the corrected emission $I_F/(1 - 10^{-A})$, where A is the absorbance, would be an horizontal line because the phenanthrene fluorescence quantum yield is constant (the amount of photons emitted by phenanthrene is directly proportional to the amount of photons adsorbed). However, in our data the corrected emission decreases approximately exponentially up to a concentration of $\text{p(DMA}_{50\text{K}}/\text{PHE}_3/\text{DO}_{10})$ close to $4.5 \times 10^{-7} \text{ g/mL}$. At this concentration the hydrodynamic diameter of the polymer-coated PNP-AN is ca. 135 nm (cf. Figure 2). Since the PBMA nanoparticle core has a hydrodynamic diameter of 129 nm, the polymer shell coating has a thickness of approximately 6 nm, very close to the limit to which FRET occurs for the phenanthrene–anthracene pair.¹⁸

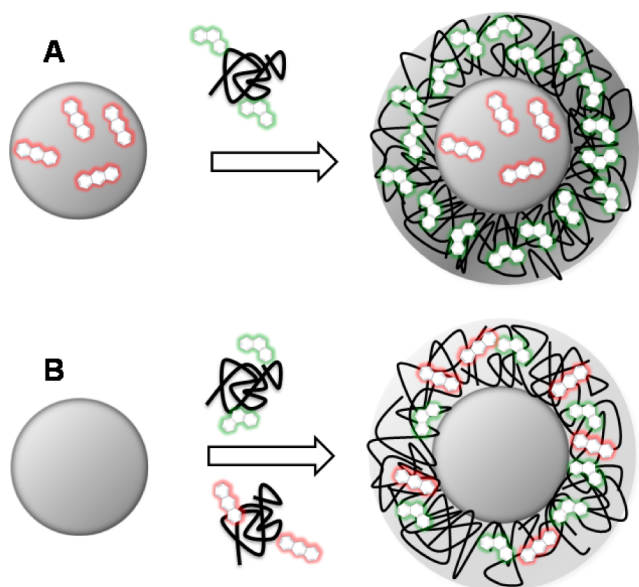


Figure 5. FRET from phenanthrene- (green) labeled chains, p(DMA_{50K}/PHE₃/DO₁₀), to anthracene (red) in either PNP-AN (A) or p(DMA_{50K}/AN₂/DO₁₈) anthracene-labeled chains adsorbed onto PNP (B).

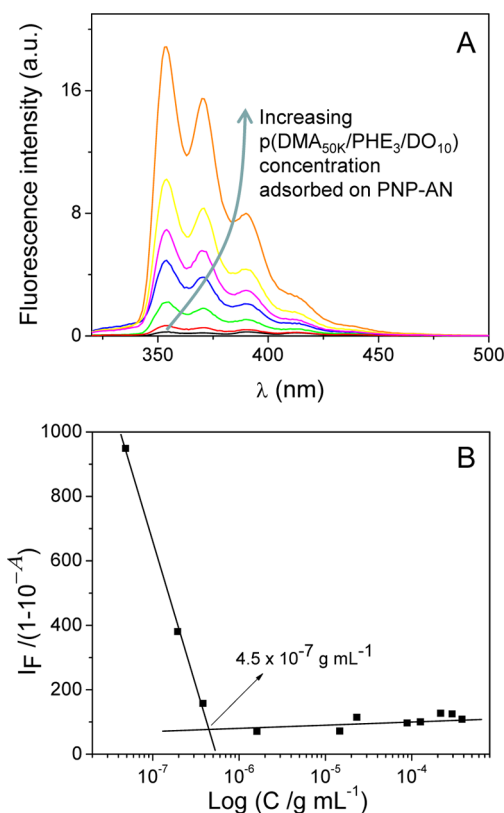


Figure 6. (A) Emission spectra of p(DMA_{50K}/PHE₃/DO₁₀) phenanthrene-labeled copolymer adsorbed onto PNP-AN (0.019 wt % in water), with excitation at 295 nm, for different concentrations of the Phe-labeled polymer: (black —) 1.46×10^{-5} g/mL, (red —) 2.30×10^{-5} g/mL, (green —) 8.80×10^{-5} g/mL, (blue —) 9.2×10^{-5} g/mL, (magenta —) 2.16×10^{-4} g/mL, (yellow —) 3.83×10^{-4} g/mL, and (orange —) 4.19×10^{-4} g/mL. (B) Fluorescence intensity at 355 nm corrected with the light absorbed by the phenanthrene dyes in the copolymer, $I_F / (1 - 10^{-A})$.

The change in energy transfer as a function of concentration is also observed in the donor fluorescence decay profiles (Figure 7A), which show a strong decrease in the phenanthrene

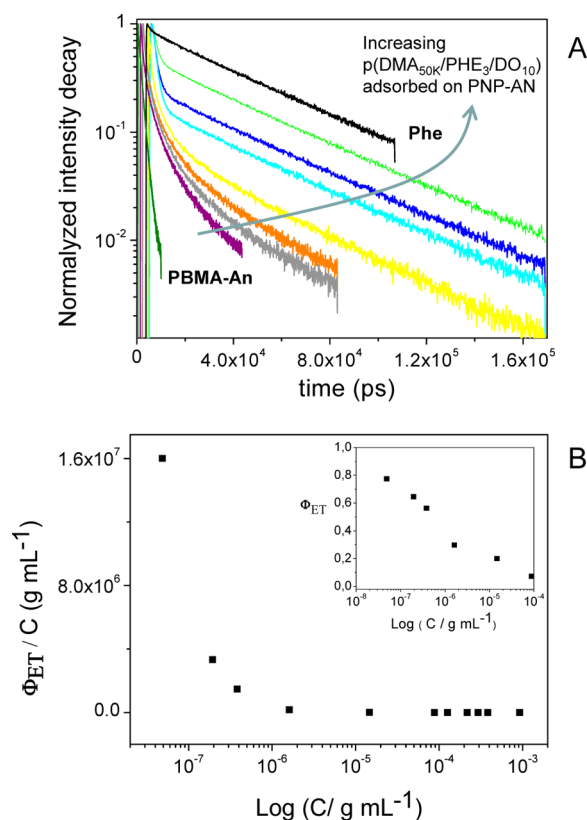


Figure 7. (A) Intensity decays (measured at 350 nm, using 295 nm excitation light) for p(DMA_{50K}/PHE₃/DO₁₀) adsorbed on PNP-AN (0.019 wt %), at polymer concentrations 8.82×10^{-5} to 4.84×10^{-8} g/mL. Phenanthrene decay in the absence of PNP-AN nanoparticles (black) and for increasing concentrations of p(DMA_{50K}/PHE₃/DO₁₀) adsorbed on PNP-AN: (green) 8.82×10^{-5} g/mL, (blue) 6.0×10^{-5} g/mL, (turquoise) 2.31×10^{-5} g/mL, (yellow) 1.61×10^{-6} g/mL, (orange) 3.80×10^{-7} g/mL, (gray) 1.94×10^{-7} g/mL, and (purple) 4.84×10^{-8} g/mL. The decay of PNP-AN (0.019 wt %) is also shown (olive). (B) Efficiency of the energy transfer calculated for p(DMA_{50K}/PHE₃/DO₁₀) adsorbed on PNP-AN (0.019 wt %), divided by the concentration of p(DMA_{50K}/PHE₃/DO₁₀).

lifetime for low phenanthrene concentrations (where all the polymer is located near the nanoparticle surface, at close distance from the energy-acceptor anthracene). For higher p(DMA_{50K}/PHE₃/DO₁₀) concentrations, most phenanthrene lies far from the surface of the anthracene-labeled particle, contributing to the fluorescence decay component that corresponds to the unquenched lifetime of phenanthrene.

The efficiency of energy transfer can be calculated as

$$\Phi_{ET} = 1 - \frac{\tau}{\tau_0} \quad (2)$$

where τ/τ_0 is the ratio of the average decay lifetime of phenanthrene (donor) with and without anthracene (acceptor).⁴⁶ The efficiency of energy transfer for different polymer concentrations is shown in the inset of Figure 7B, with Φ_{ET} starting at 77% when all phenanthrene-labeled polymer is very close to the surface. As the amount of adsorbed polymer increases, the average distance of the additional phenanthrene

dyes to the particle is larger and the efficiency of FRET decreases. Eventually, Φ_{ET} tends to zero as the amount of phenanthrene next to the particle surface becomes irrelevant compared to the total amount of phenanthrene on the adsorbed polymer shell. To account for the trivial decrease in Φ_{ET} due to the increase in phenanthrene concentration, we divide this efficiency by the polymer concentration (Figure 7B). This ratio decreases to zero (no effect of energy transfer) around 6×10^{-7} g/mL of polymer (close to the value obtained from the fluorescence spectra of the coated particles, Figure 6).

In the experiment previously described, FRET occurs only close to the particle surface, thus limiting the ability of this technique to provide information on the morphology of the polymer adsorbed onto the particle. In order to characterize this layer, we designed a different experiment, where we adsorb both p(DMA_{50K}/PHE₃/DO₁₀) donor-labeled polymer and p(DMA_{50K}/AN₂/DO₁₈) acceptor-labeled polymer onto unlabeled PNPs at total polymer concentration well below the CAC of the polymers, so that FRET occurs only within the spherical shell formed by the adsorbed polymer layer (Figure 5B).¹⁸ While the CAC is known to change with the hydrophobic content of the polymers, the difference between our donor- and acceptor-labeled polymers is not expected to have a significant effect.³³ To test this hypothesis, mixtures with different ratios of p(DMA_{50K}/PHE₃/DO₁₀) and p(DMA_{50K}/AN₂/DO₁₈) in water, with total polymer concentrations of 1.18×10^{-5} g/mL (below the CAC) and 7.25×10^{-4} g/mL (above the CAC), were adsorbed onto PNP (0.0019 wt %). The diameter of the coated particles was not affected by the difference in hydrophobic group content of the two polymers (Figure 8),

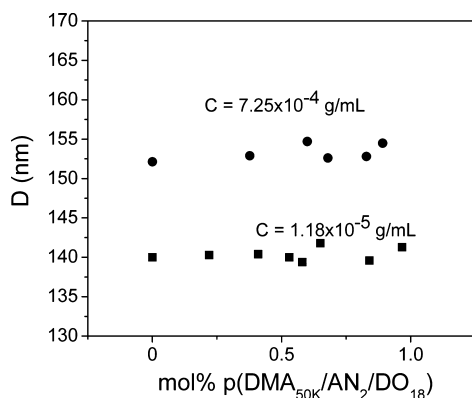


Figure 8. Hydrodynamic diameter for mixtures of p(DMA_{50K}/PHE₃/DO₁₀) and p(DMA_{50K}/AN₂/DO₁₈) adsorbed onto PNP (0.019 wt %) for total polymer concentrations of (■) 1.18×10^{-5} g/mL and (●) 7.25×10^{-4} g/mL, as a function of p(DMA_{50K}/AN₂/DO₁₈) molar ratio.

with the hydrodynamic diameter showing constant values within experimental error. However, we observed that, only for polymer concentrations lower than the polymer CAC in water, we had complete adsorption of the polymer on the surface of the nanoparticles: after the coated PNPs were centrifuged at 15 000 rpm and filtrated with a 0.1 μ m membrane, the resulting supernatant shows no phenanthrene or anthracene emission.

If the dyes were randomly distributed in the adsorbed shell, we would expect the shell thickness calculated from the analysis of the fluorescence decays to coincide with the value determined by DLS. Otherwise, if the hydrophobic groups were preferentially adsorbed onto the particles surface, the shell

thickness determined by FRET would be thinner than the one determined by DLS. In Figure 9 we show the donor intensity

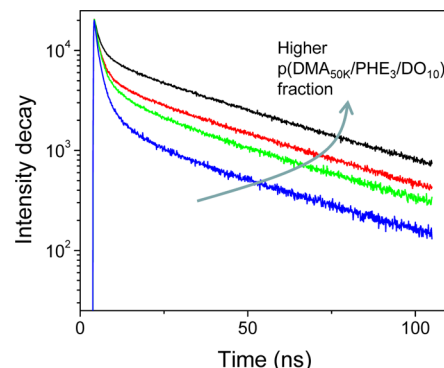


Figure 9. Intensity decay curves for mixtures of p(DMA_{50K}/PHE₃/DO₁₀) and p(DMA_{50K}/AN₂/DO₁₈) adsorbed onto PNP (0.019 wt %) at a total polymer concentration of 1.18×10^{-5} g/mL. The weight ratios of phenanthrene- to anthracene-labeled polymer are 1.38 (black), 0.71 (red), 0.19 (green), and 0.08 (blue).

decay curves ($\lambda_{exc} = 295$ nm, $\lambda_{em} = 350$ nm) for samples of coated PNP with a total concentration of hydrophobically modified copolymer equal to 1.18×10^{-5} g/mL and different ratios of p(DMA_{50K}/PHE₃/DO₁₀) and p(DMA_{50K}/AN₂/DO₁₈). A strong increase in energy transfer from the phenanthrene to the anthracene groups (faster decay curves) is detected for the mixtures with higher p(DMA_{50K}/AN₂/DO₁₈) molar fractions.

The decay curves shown in Figure 9 contain information on the distribution of the anthracene- and phenanthrene-labeled polymers adsorbed on the nanoparticle surface. To extract this information we need to analyze the kinetics of Förster resonance energy transfer (FRET)⁴⁷ from phenanthrene to anthracene. For a dipole–dipole coupling mechanism, the rate of energy transfer $w(r)$ between a donor and an acceptor depends heavily on their separation distance r

$$w(r) = \frac{3\kappa^2}{2\tau_D} \left(\frac{R_0}{r} \right)^6 \quad (3)$$

where τ_D is the unquenched donor fluorescence lifetime, R_0 is the critical Förster distance determined as $R_0 = (2.3 \pm 0.1)$ nm for the phenanthrene–anthracene pair,^{48,49} and κ^2 is a dimensionless parameter related to the relative orientation of the donor and acceptor transition dipole moments. According to the distribution model for energy transfer in spherical systems,^{49–51} the donor decay function after a delta-pulse excitation will be given by

$$I_D(t) = \exp\left(-\frac{t}{\tau_D}\right) \int_{V_s} C_D(r_D) \phi(t, r_D) r_D^2 dr_D \quad (4)$$

$$\phi(t, r_D) = \exp\left(-\frac{2\pi}{r_D} \int_{R_D}^{\infty} \{1 - \exp[-w(r)t]\} \left[\int_{r_D-r}^{r_D+r} C_A(r_A) r_A dr \right] dr\right) \quad (5)$$

where V_s is the volume of the adsorption shell where donors and acceptors are distributed, R_c is the minimum distance between donor and acceptor, and the distribution functions of

donor and acceptor dyes in the adsorbed shell, $C_D(r)$ and $C_A(r)$, are modeled using a hyperbolic tangent function, modified to account for the spherical shell geometry of the nanoparticle.^{37,46,52–57} The experimental donor fluorescence decay curves are analyzed by simulating the donor survival probability curves using this model and then comparing the simulated curves with the experimental donor fluorescence decay curves (Supporting Information).

In Figure 10 we show the reduced χ^2 resulting from fitting the simulated curves to the donor decay curve obtained for a

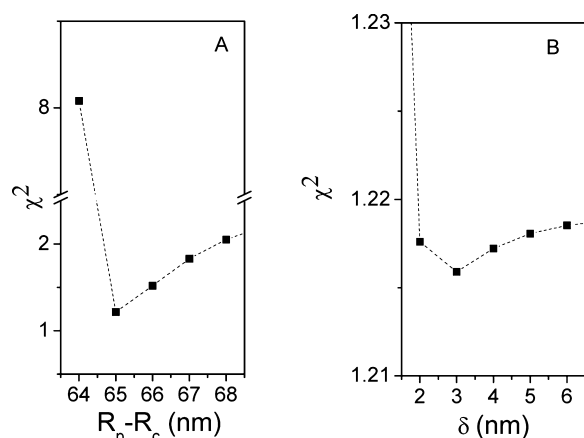


Figure 10. Reduced χ^2 from fitting the simulated fluorescence donor decay curves to the experimental decays obtained for a total polymer concentration of 1.18×10^{-5} g/mL with a weight ratio of phenanthrene- to anthracene-labeled polymers of 1.38, in a 0.019 wt % PNP dispersion.

total polymer concentration of 1.18×10^{-5} g/mL with a weight ratio of phenanthrene- to anthracene-labeled polymers of 1.38, in a 0.0019 wt % PNP dispersion. The same fitting procedure was used for different ratios of anthracene- to phenanthrene-labeled polymers, yielding an average coated particle radius of $R_p = (65.0 \pm 0.5)$ nm with an interface smoothness parameter of $\delta = (3.0 \pm 0.5)$ nm. For these values, the particle radius that includes 99% of the distribution function (Supporting Information) is $R_{\text{FRET}} = R_p + \delta = (68 \pm 0.7)$ nm. This value corresponds to a shell of thickness 4.5 nm ($R_c = 63.5$ nm) containing the hydrophobic dyes on the adsorbed polymer. The radius of the coated particle R_{FRET} is only slightly smaller than the hydrodynamic radius measured by DLS, $R_H = 70.0$ nm, indicating that the dyes (and therefore all the hydrophobic side groups) are not located at the particle interface as predicted by the hairy carpet model but mostly distributed across the adsorbed layer, indicating that this is most probably held together by interaction between hydrophobic groups of different chains.

Influence of Polymer Chain Length. To study the influence of polymer chain length on the adsorption onto the PNPs, we used a polymer with similar structure and composition to the previously studied but with a molecular weight five times larger (250k), and labeled with pyrene, $p(\text{DMA}_{250\text{K}}/\text{PY}_{12}/\text{DO}_{38})$. This polymer was added to a dispersion of the PNPs, previously coated with a shorter polymer, $p(\text{DMA}_{50\text{K}}/\text{PHE}_3/\text{DO}_{10})$ (cartoon in Figure 11).

We started by measuring the DLS of the nanoparticles coated with increasing concentration of the larger polymer (250k), which yielded increasing hydrodynamic diameters, larger than those obtained for the same particles coated with the smaller

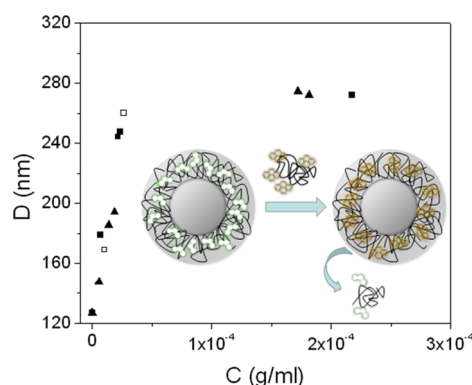


Figure 11. Hydrodynamic diameter of $p(\text{DMA}_{250\text{K}}/\text{PY}_{12}/\text{DO}_{38})$ -coated PNP determined by DLS (■) and FCS (□). When PNPs previously coated with $p(\text{DMA}_{50\text{K}}/\text{PHE}_3/\text{DO}_{10})$ were mixed with different concentrations of $p(\text{DMA}_{250\text{K}}/\text{PY}_{12}/\text{DO}_{38})$ (cartoon), the final hydrodynamic diameters of the PNP (▲) are similar to those obtained by coating bare PNPs with $p(\text{DMA}_{250\text{K}}/\text{PY}_{12}/\text{DO}_{38})$.

$p(\text{DMA}_{50\text{K}}/\text{PHE}_3/\text{DO}_{10})$ polymers (filled squares in Figure 11). We also carried out experiments of FCS at two different concentrations of $p(\text{DMA}_{250\text{K}}/\text{PY}_{12}/\text{DO}_{38})$, 1.02×10^{-5} and 2.63×10^{-5} g/mL, and the diameters obtained, 169 and 260 nm (open squares in Figure 11), are in good agreement with those obtained by DLS.

In order to characterize the displacement of adsorbed hydrophobically modified polymer chains by larger chains, we adsorbed $p(\text{DMA}_{50\text{K}}/\text{PHE}_3/\text{DO}_{10})$ onto PNP and, after stabilization, added the longer $p(\text{DMA}_{250\text{K}}/\text{PY}_{12}/\text{DO}_{38})$ chains. The hydrodynamic diameters determined by DLS by adding different concentrations of $p(\text{DMA}_{250\text{K}}/\text{PY}_{12}/\text{DO}_{38})$ to $p(\text{DMA}_{50\text{K}}/\text{PHE}_3/\text{DO}_{10})$ -coated PNP (triangles in Figure 11) are very similar to those obtained by coating bare PNP with the same concentrations of $p(\text{DMA}_{250\text{K}}/\text{PY}_{12}/\text{DO}_{38})$, indicating that the initially adsorbed smaller chains are possibly displaced by the larger chains. In order to clarify this, we performed an experiment where the fluorescence of the same samples was compared before and after they were centrifuged (at 21 000 g) and filtered (with $0.1 \mu\text{m}$ filters). Since the emission spectra of phenanthrene and pyrene only overlap for wavelengths above 360 nm, we can observe the fluorescence of phenanthrene at 350 nm, separated from that of pyrene (Figure SI-2, Supporting Information). The emission spectra of the mixture before filtering and of the supernatant after filtering (Figure SI-3, A and B, Supporting Information) show that the initially adsorbed phenanthrene-labeled $p(\text{DMA}_{50\text{K}}/\text{PHE}_3/\text{DO}_{10})$ is displaced by the preferentially adsorbed pyrene-labeled $p(\text{DMA}_{250\text{K}}/\text{PY}_{12}/\text{DO}_{38})$. In fact, when 7.11×10^{-6} g/mL of $p(\text{DMA}_{250\text{K}}/\text{PY}_{12}/\text{DO}_{38})$ is added to the coated particles, centrifugation and filtration yielded a supernatant showing the same amount of phenanthrene as initially adsorbed, while the amount of detected pyrene decreases because the pyrene labeled polymer stays adsorbed in the particles (we followed the amount of particles present in the dispersion by their scattering originating from the second harmonic of the excitation wavelength, at 600 nm).

When we increased the concentration of $p(\text{DMA}_{250\text{K}}/\text{PY}_{12}/\text{DO}_{38})$ added to the coated particles to 1.46×10^{-6} g/mL (Figure SI-3 B, Supporting Information), we observed the same effect, but in this case the supernatant contains the phenanthrene-labeled polymer and the excess pyrene-labeled polymer (its concentration is above the maximum adsorbed

concentration), which form mixed polymer aggregates where energy transfer occurs from phenanthrene to pyrene (with the consequent reduction in phenanthrene fluorescence intensity at 350 nm).

We also measured the fluorescence decay curves of the supernatants at the phenanthrene emission wavelength (Figure SI-4, Supporting Information). For the lower concentration of p(DMA_{250K}/PY₁₂/DO₃₈), 7.11×10^{-6} g/mL, the decay curve coincides with that of p(DMA_{50K}/PHE₃/DO₁₀) alone, because all the pyrene-labeled polymer stays adsorbed at the particles and the displaced phenanthrene-labeled chains are dissolved in the supernatant. However, for the experiment with 1.46×10^{-4} g/mL of p(DMA_{250K}/PY₁₂/DO₃₈), some of the pyrene-labeled polymer is not adsorbed in the particle and is thus present in the supernatant. These chains aggregate with p(DMA_{50K}/PHE₃/DO₁₀) to form mixed aggregates in which the phenanthrene decay curves become nonexponential due to Förster resonance energy transfer from phenanthrene to pyrene.

CONCLUSIONS

We prepared a fluorescent amphiphilic polymer of *N,N*-dimethylacrylamide (DMA) with hydrophobic (dodecyl, DO) and fluorescent (pyrene, PY; phenanthrene, PHE; or anthracene, AN) side groups, from a reactive random copolymer of DMA and *N*-acryloxysuccinimide (NAS) with $M_n \approx 50k$, using reversible addition–fragmentation chain transfer (RAFT) polymerization. The fluorescent hydrophobically modified pDMA chains adsorb efficiently onto model polymer nanoparticles of poly(butyl methacrylate) with ca. 130 nm diameter, with the adsorbed layer increasing rapidly with pDMA concentration up to ca. 140 nm, and then more slowly to a limiting value of 154 nm, which corresponds to a polymer shell thickness of ca. 12 nm—much larger than the hydrodynamic diameter of a single polymer chain, $D_h^{UNI} = 3.4$ nm. This points to a multilayer type adsorption, probably held together by the hydrophobic side groups of the polymer chain. In fact, by analyzing the Förster resonance energy transfer (FRET) between adsorbed PHE- and AN-labeled PDMA chains, we conclude that the hydrophobic fluorescent groups are distributed over all the adsorbed layer, not only at the nanoparticle surface.

Finally, we observed that hydrophobically modified PY-labeled ($M_n \approx 250k$) PDMA chains with five times the molecular weight of the analogous PHE-labeled ($M_n \approx 50k$) chains efficiently substitute the previously adsorbed smaller chains.

ASSOCIATED CONTENT

Supporting Information

Formalism of Förster resonance energy transfer (FRET) kinetics for donor and acceptor dyes distributed in the polymer layer adsorbed onto a spherical particle and methods followed for the analysis of the experimental donor fluorescence decay curves; spectra and donor fluorescence decay curves related to the influence of the polymer chain length on the adsorption process. This material is available free of charge via the Internet at <http://pubs.acs.org>.

AUTHOR INFORMATION

Corresponding Author

*E-mail: (farinha@ist.utl.pt) (J.P.S.F.); (gema.marcelo@ictp.csic.es) (G.M.).

Notes

The authors declare no competing financial interest.

ACKNOWLEDGMENTS

This work was partially supported by Fundação para a Ciência e a Tecnologia (FCT, Portugal) and COMPETE (FEDER) within project PTDC/CTM-NAN/115110/2009. Dr. Aleksander Fedorov (CQFM-IN) is acknowledged for technical assistance with the picosecond lifetime measurements. G.M. also thanks FCT for a postdoc grant (SFRH/BPD/42470/2007).

REFERENCES

- (1) (a) Fleer, G. J.; Cohen Stuart, M. A.; Scheutjens, J. M. H. M.; Cosgrove, T.; Vincent, B. In *Polymers at Interfaces*; Chapman & Hall: London, U.K., 1993. (b) Qiu, D.; Cosgrove, T.; Revell, P.; Howell, I. Poly(ethylene oxide) Adsorption on Polystyrene Latex Particles in the Presence of Poly(styrenesulfonate sodium). *Macromolecules* **2009**, *42*, 547–552.
- (2) Wagner, N. J.; Brady, J. F. Shear Thickening in Colloidal Dispersions. *Phys. Today* **2009**, *62*, 27–32.
- (3) Christensen, P. V.; Keiding, K. The Use of Dielectric Spectroscopy for the Characterization of Polymer-Induced Flocculation of Polystyrene Particles. *J. Colloid Interface Sci.* **2008**, *327*, 362–369.
- (4) Gregory, J.; Barany, S. Adsorption and Flocculation by Polymers and Polymer Mixtures. *Adv. Colloid Interface Sci.* **2011**, *169*, 1–12.
- (5) (a) Napper, D. H. *Polymeric Stabilization of Colloidal Dispersions*; Academic Press: London, U.K., 1983. (b) Fleer, G. J.; Cohen Stuart, M. A.; Scheutjens, J. M. H. M.; Cosgrove, T.; Vincent, B. *Polymers at Interfaces*; Chapman & Hall: London, U.K., 1993. (c) Russel, W. B.; Saville, D. A.; Schowalter, W. R. *Colloidal Dispersions*; Cambridge University Press: New York, 1989. (d) Vincent, B. The Effect of Adsorbed Polymers on the Stability of Dispersions. *Adv. Colloid Interface Sci.* **1974**, *4*, 193–277.
- (6) Oulanti, O.; Widmaier, J.; Pefferkorn, E.; Champ, S.; Auweter, H. Destabilization of Polystyrene Latex Particles Induced by Adsorption of Polyvinylamine: Mass, Size and Structure Characteristics of the Growing Aggregates. *J. Colloid Interface Sci.* **2006**, *294*, 95–103.
- (7) (a) Lafuma, F.; Wong, K.; Cabane, B. Bridging of Colloidal Particles Through Adsorbed Polymers. *J. Colloid Interface Sci.* **1991**, *143*, 9–21. (b) Spalla, O.; Cabane, B. Growth of Colloidal Aggregates Through Polymer Bridging. *Colloid Polym. Sci.* **1993**, *271*, 357–371. (c) Spalla, O. Nanoparticle Interactions with Polymers and Polyelectrolytes. *Curr. Opin. Colloid Interface Sci.* **2002**, *7*, 179–185. (d) Wang, T. K.; Audebert, R. Flocculation Mechanisms of a Silica Suspension by Some Weakly Cationic Polyelectrolytes. *J. Colloid Interface Sci.* **1987**, *119*, 459–465. (e) Fleer, G. J.; Scheutjens, J. M. H. M. Interaction Between Adsorbed Layers of Macromolecules. *J. Colloid Interface Sci.* **1986**, *111*, 504–515. (f) Wong, K.; Cabane, B.; Duplessix, R. Interparticle Distances in Flocs. *J. Colloid Interface Sci.* **1988**, *123*, 466–481. (g) Durand-Piana, G.; Lafuma, F.; Audebert, R. Flocculation and Adsorption Properties of Cationic Polyelectrolytes Toward Na-Montmorillonite Dilute Suspensions. *J. Colloid Interface Sci.* **1987**, *119*, 474–480. (h) Wong, K.; Lixon, P.; Lafuma, F.; Lindner, P.; Aguerre-Charriol, O.; Cabane, B. Intermediate Structures in Equilibrium Flocculation. *J. Colloid Interface Sci.* **1992**, *153*, 55–72.
- (8) (a) Wijmans, C. M.; Zhulina, E. B. Polymer Brushes at Curved Surfaces. *Macromolecules* **1993**, *26*, 7214–7224. (b) Aubouy, A.; Raphael, E. Scaling Descriptions of a Colloidal Particle Clothed with Polymers. *Macromolecules* **1998**, *31*, 4357–4363. (c) Ji, H.; Hone, D. Polymer Adsorption on Rough Surfaces. 2. Good Solvent Conditions. *Macromolecules* **1988**, *21*, 2600–2605. (d) Skau, K. I.; Blokhuis, E. M. Polymer Adsorption on Curved Surfaces: Finite Chain Length Corrections. *Macromolecules* **2003**, *36*, 4637–4645. (e) Farinha, J. P. S.; d'Oliveira, J. M. R.; Martinho, J. M. G.; Xu, R.; Winnik, M. A. Structure in Tethered Chains: Polymeric Micelles and Chains

Anchored on Polystyrene Latex Spheres. *Langmuir* **1998**, *14*, 2291–2296.

(9) Frantz, P.; Granik, S. Kinetics of Polymer Adsorption and Desorption. *Phys. Rev. Lett.* **1991**, *66*, 899–902.

(10) (a) Frantz, P.; Granik, S. Infrared Dichroism, Chain Flattening, and the Bound Fraction Histogram in Adsorbed Poly(methyl methacrylate) Layers. *Macromolecules* **1995**, *28*, 6915–6925. (b) Johnson, H. E.; Granik, S. New Mechanism of Nonequilibrium Polymer Adsorption. *Science* **1992**, *255*, 966–968.

(11) Dickinson, E. Milk Protein Interfacial Layers and the Relationship to Emulsion Stability and Rheology. *Colloids Surf., B* **2001**, *20*, 197–210.

(12) (a) Munch, M. R.; Gast, A. P. Kinetics of Block Copolymer Adsorption on Dielectric Surfaces from a Selective Solvent. *Macromolecules* **1990**, *23*, 2313–2320. (b) Xu, R. L.; Winnik, M. A.; Riess, G.; Chu, B.; Croucher, M. D. Micellization of Polystyrene–Poly(ethylene oxide) Block Copolymers in Water. 5. A Test of the Star and Mean-Field Models. *Macromolecules* **1992**, *25*, 644–652.

(13) (a) Min, G. K.; Bevan, M. A.; Prieve, D. C.; Patterson, G. D. Light Scattering Characterization of Polystyrene Latex With and Without Adsorbed Polymer. *Colloids Surf., A* **2002**, *202*, 9–21. (b) Biasio, A. D.; Bordi, F.; Cametti, C. Effect of Polymer Adsorption on PEO-Coated Latex Particles During Salt Induced Aggregation. *Colloids Surf., A* **1999**, *160*, 189–198. (c) Napper, D. H. *Polymeric Stabilization of Colloidal Dispersion*; Academic: New York, 1983. (d) Walz, J. Y. Effect of Polydispersity on the Depletion Interaction Between Colloidal Particles. *J. Colloid Interface Sci.* **1996**, *178*, 505–513. (e) Smith, N. J.; Williams, P. A. Depletion Flocculation of Polystyrene Lattices by Water Soluble Polymers. *J. Chem. Soc., Faraday Trans.* **1995**, *91*, 1483–1489. (f) Liang, W.; Tadros, T. F.; Luckham, P. F. Flocculation of Sterically Stabilized Polystyrene Latex Particles by Adsorbing and Nonadsorbing Poly(acrylic acid). *Langmuir* **1994**, *10*, 441–446.

(14) (a) Oberdisse, J. Adsorption and Grafting on Colloidal Interfaces Studied by Light Scattering Techniques. *Curr. Opin. Colloid Interface Sci.* **2007**, *12*, 3–8. (b) Likos, C. N.; Vaynberg, K. A.; Lowen, H.; Wagner, N. J. Colloidal Stabilization by Adsorbed Gelatin. *Langmuir* **2000**, *16*, 4100–4108. (c) Vaynberg, K. A.; Wagner, N. J.; Sharma, R.; Martic, P. Structure and Extent of Adsorbed Gelatin on Acrylic Latex and Polystyrene Colloidal Particles. *J. Colloid Interface Sci.* **1998**, *205*, 131–140.

(15) Wen, Y. H.; Lin, P.-C.; Lee, C. Y.; Hua, C. C.; Lee, T.-C. Reduced Colloidal Repulsion Imparted by Adsorbed Polymer of Particle Dimensions. *J. Colloid Interface Sci.* **2010**, *349*, 134–141.

(16) Uemura, Y.; Macdonald, P. M. NMR Diffusion and Relaxation Time Studies of HEUR Associating Polymer Binding to Polystyrene Latex. *Macromolecules* **1996**, *29*, 63–69.

(17) Char, K.; Frank, C. W.; Gast, A. P. Fluorescence Studies of Polymer Adsorption. 3. Adsorption of Pyrene-End-Labeled Poly(ethylene glycol) on Colloidal Polystyrene Particles. *Langmuir* **1989**, *5*, 1335–1340.

(18) Farinha, J. P. S.; Martinho, J. M. G. Resonance Energy Transfer in Polymer Nanodomains. *J. Phys. Chem. C* **2008**, *112*, 10591–10601.

(19) Chiefari, J.; Chong, Y. K.; Ercole, F.; Krstina, J.; Jeffery, J.; Le, T. P. T.; Mayadunne, R. T. A.; Meijs, G. F.; Moad, C. L.; Moad, G.; Rizzardo, E.; Thang, S. H. Living Free Radical Polymerization by Reversible Addition–Fragmentation Chain Transfer. The RAFT Process. *Macromolecules* **1998**, *31*, 5559–5562.

(20) Beija, M.; Charreyre, M.-T.; Martinho, J. M. G. Dye-Labelled Polymer Chains at Specific Sites: Synthesis By Living/Controlled Polymerization. *Prog. Polym. Sci.* **2011**, *36*, 568–602.

(21) Moad, G.; Chiefari, J.; Chong, B. Y. K.; Krstina, J.; Mayadunne, R. T. A.; Postma, A.; Rizzardo, E.; Thang, S. H. Living Free Radical Polymerization with Reversible Addition–Fragmentation Chain Transfer (The Life of RAFT). *Polym. Int.* **2000**, *49*, 993–1000.

(22) Relógio, P.; Charreyre, M.-T.; Farinha, J. P. S.; Martinho, J. M. G.; Pichot, C. Well-Defined Polymer Precursors Synthesized by RAFT Polymerization of *N,N*-Dimethylacrylamide/*N*-Acryloxysuccinimide: Random and Block Copolymers. *Polymer* **2004**, *45*, 8639–8649.

(23) Arshady, R. Polymers Synthesis Via Activated Esters: A New Dimension of Creativity in Macromolecular Chemistry. *Adv. Polym. Sci.* **1994**, *111*, 1–41.

(24) (a) Kepecek, J.; Sprinel, L.; Bazilova, H.; Vacik, J. Biological Tolerance of Poly(*N*-substituted methacrylamides). *J. Biomed. Mater. Res.* **1971**, *5*, 197–205. (b) Ferruti, P.; Domini, I.; Barbucci, R.; Beni, M.; Dispensa, E.; Sancasciani, S.; Marchisio, M.; Tanzi, M. Heparin Adsorbing Capacities at Physiological pH of Three Poly(amido-amine) Resins and of Poly(amido-amine)-Surface-Grafted Glass Microspheres. *Biomaterials* **1983**, *4*, 218–221.

(25) D'Agosto, F.; Charreyre, M.-T.; Pichot, C. Side-Product of *N*-Acryloyloxysuccinimide Synthesis or Useful New Bifunctional Monomer? *Macromol. Biosci.* **2001**, *1*, 322–328.

(26) Favier, A.; Charreyre, M.-T.; Chaumont, P.; Pichot, C. Study of the RAFT Polymerization of a Water-Soluble Bisubstituted Acrylamide Derivative. 1. Influence of the Dithioester Structure. *Macromolecules* **2002**, *35*, 8271–8280.

(27) Afonso, C. A. M.; Farinha, J. P. S. Synthesis of 4-Aryl-butylamine Fluorescent Probes. *J. Chem. Res., Synop.* **2002**, *11*, 584–587.

(28) Piçarra, S.; Afonso, C. A. M.; Kurteva, V. B.; Fedorov, A.; Martinho, J. M. G.; Farinha, J. P. S. The Influence of Nanoparticle Architecture on Latex Film Formation and Healing Properties. *J. Colloid Interface Sci.* **2012**, *368*, 21–33.

(29) Winnik, F. M. Fluorescence Studies of Aqueous Solutions of Poly(*N*-isopropylacrylamide) below and above Their LCST. *Macromolecules* **1990**, *23*, 233–242.

(30) Piçarra, S.; Relógio, P.; Afonso, C. A. M.; Martinho, J. M. G.; Farinha, J. P. S. Coil-Globule Transition of Poly(dimethyl acrylamide): Fluorescence and Light Scattering Study. *Macromolecules* **2003**, *36*, 8119–8129.

(31) Chiefari, J.; Chong, Y. K.; Ercole, F.; Krstina, J.; Jeffery, J.; Le, T. P. T.; Mayadunne, R. T. A.; Meijs, G. F.; Moad, C. L.; Moad, G.; Rizzardo, E.; Thang, S. H. Living Free-Radical Polymerization by Reversible Addition–Fragmentation Chain Transfer: The RAFT Process. *Macromolecules* **1998**, *31*, 5559–5562.

(32) Beija, M.; Relógio, P.; Charreyre, M.-T.; Gonçalves da Silva, A. M.; Brogueira, P.; Farinha, J. P. S.; Martinho, J. M. G. Thin Films of Hydrophobically-Modified Poly(*N,N*-Dimethylacrylamide). *Langmuir* **2005**, *21*, 3940–3949.

(33) Relógio, P.; Martinho, J. G. M.; Farinha, J. P. S. Effect of Surfactant on the Intra- and Intermolecular Association of Hydrophobically Modified Poly(*N,N*-dimethylacrylamide). *Macromolecules* **2005**, *38*, 10799–10811.

(34) Farinha, J. P. S.; Relógio, P.; Charreyre, M.-T.; Prazeres, T. J. V.; Martinho, J. G. M. Understanding and Avoiding Fluorescence Quenching in Polymers Obtained by RAFT. *Macromolecules* **2007**, *40*, 4680–4691.

(35) Mukerjee, P.; Mysels, K. J. *Critical Micelle Concentrations of Aqueous Surfactant Systems*; National Standard Reference Data Systems: Washington, DC, 1971.

(36) Benrraou, M.; Bales, B. L.; Zana, R. Effect of the nature of the counterion on the properties of anionic surfactants. 1. Cmc, ionization degree at the cmc and aggregation number of micelles of sodium, cesium, tetramethylammonium, tetraethylammonium, tetrapropylammonium, and tetrabutylammonium dodecyl sulfates. *J. Phys. Chem. B* **2003**, *107*, 13432–13440.

(37) Ye, S.; Farinha, J. P. S.; Oh, J. K.; Winnik, M. A.; Wu, C. Polymer Diffusion in PBMA Latex Films Using a Polymerizable Benzophenone Derivative as an Energy Transfer Acceptor. *Macromolecules* **2003**, *36*, 8749–8769.

(38) Zhou, C. L.; Winnik, M. A.; Jao, T. C. Synthesis and Characterization of Nonaqueous Dispersion Particles with Photolabile *N*-Heptadecylphenacyl Ester Stabilizer Chains. *J. Polym. Sci., Part A: Polym. Chem.* **2001**, *39*, 2642–2657.

(39) In *Photon Correlation Spectroscopy and Velocimetry*; Cummins, H. Z., Pike, E. R., Eds.; Plenum Press: New York, 1977.

(40) Ribeiro, T.; Baleizão, C.; Farinha, J. P. S. Synthesis and Characterization of Perylenediimide Labeled Core–Shell Hybrid

Silica–Polymer Nanoparticles. *J. Phys. Chem. C* **2009**, *113*, 18082–18090.

(41) Farinha, J. P. S.; Martinho, J. M. G.; Pogliani, L. Non-Linear Least-Squares and Chemical Kinetics. An Improved Method to Analyze Monomer-Excimer Decay Data. *J. Math. Chem.* **1997**, *21*, 131–139.

(42) Prazeres, T. J. V.; Beija, M.; Fernandes, F. V.; Marcelino, P. G. A.; Farinha, J. P. S.; Martinho, J. M. G. Determination of the Critical Micelle Concentration of Surfactants and Amphiphilic Block Copolymers Using Coumarin 153. *Inorg. Chim. Acta* **2012**, *381*, 181–187.

(43) Humpolicková, J.; Prochazka, K.; Hof, M.; Tuzar, Z.; Šýpírková, M. Fluorescence Correlation Spectroscopy Using Octadecylrhodamine B as a Specific Micelle-Binding Fluorescent Tag; Light Scattering and Tapping Mode Atomic Force Microscopy Studies of Amphiphilic Water-Soluble Block Copolymer Micelle. *Langmuir* **2003**, *19*, 4111–4119.

(44) (a) Ottewill, R. H. *Langmuir* **1989**, *5*, 4–11. (b) Zackrisson, M.; Stradner, A.; Schurtenberger, P.; Bergenholtz, J. Small-Angle Neutron Scattering on a Core–Shell Colloidal System: A Contrast-Variation Study. *Langmuir* **2005**, *21*, 10835–10845. (c) Qiu, D.; Cosgrove, T.; Howe, A. M. Steric Interactions Between Physically Adsorbed Polymer-Coated Colloidal Particles: Soft or Hard? *Langmuir* **2007**, *23*, 475–481.

(45) Likos, C. N.; Vaynberg, K. A.; Lowen, H.; Wagner, N. J. Colloidal Stabilization by Adsorbed Gelatin. *Langmuir* **2000**, *16*, 4100–4108.

(46) Farinha, J. P. S.; Vorobyova, O.; Winnik, M. A. Interface Thickness in Blends of PBMA and PEHMA. *Macromolecules* **2000**, *33*, 5863–5873.

(47) Förster, Th. *Ann. Phys. (Leipzig)* **1948**, *2*, 55. Förster, Th. *Z. Naturforsch.* **1949**, *4a*, 321–327.

(48) Marcelo, G.; Prazeres, T.; Charreyre, M.-T.; Martinho, J. M. G.; Farinha, J. P. S. Thermoresponsive Micelles of Poly(decylacrylamide-*b*-diethylacrylamide) in Water. *Macromolecules* **2010**, *43*, 501–510.

(49) Farinha, J. P. S.; Martinho, J. M. G.; Kawagushi, S.; Yekta, A.; Winnik, M. A. Latex Film Formation Probed by Non-Radiative Energy Transfer: Effect of Grafted and Free Poly(ethylene oxide) on a Poly(*n*-butyl methacrylate) Latex. *J. Phys. Chem.* **1996**, *100*, 12552–12558.

(50) Yekta, A.; Winnik, M. A.; Farinha, J. P. S.; Martinho, J. M. G. Dipole-Dipole Electronic Energy Transfer. Fluorescence Decay Functions for Arbitrary Distributions of Donors and Acceptors in Systems with Spherical Symmetry. *J. Phys. Chem. A* **1997**, *101*, 1787–1792.

(51) Farinha, J. P. S.; Martinho, J. M. G. Electronic Energy Transfer in Restricted Geometries. Application to the Study of Spherical and Planar Interphases of Diblock Copolymer Films. *J. Lumin.* **1997**, *72*, 914–917.

(52) Farinha, J. P. S.; Martinho, J. M. G.; Charreyre, M.-T.; Pichot, C.; Winnik, M. A. Picosecond Fluorescence Studies of the Surface Morphology of Charged Polystyrene Latex Particles. *Langmuir* **2001**, *17*, 2617–2623.

(53) Pham, H.; Farinha, J. P. S.; Winnik, M. A. Crosslinking, Miscibility, and Interface Structure in Blends of Poly(2-ethylhexyl methacrylate) with its Copolymer with Methacrylic Acid. An Energy Transfer Study. *Macromolecules* **2000**, *33*, 5850–5860.

(54) Farinha, J. P. S.; Wu, J.; Winnik, M. A.; Farwaha, R.; Rademacher, J. Polymer Diffusion in Gel-Containing Poly(vinyl acetate-*co*-dibutyl acrylate) Latex Films. *Macromolecules* **2005**, *38*, 4393–4402.

(55) Fonseca, T.; Relógio, P.; Martinho, J. M. G.; Farinha, J. P. S. Preparation and Surface Characterization of Polymer Nanoparticles Designed for Incorporation into Hybrid Materials. *Langmuir* **2007**, *23*, 5727–5734.

(56) Prazeres, T.; Farinha, J. P. S.; Martinho, J. M. G. Control of Oligonucleotide Distribution on the Shell of Thermo-Responsive Polymer Nanoparticles. *J. Phys. Chem. C* **2008**, *112*, 1633–1641.

(57) (a) Farinha, J. P. S.; Schillen, K.; Winnik, M. A. Interfaces in Self-Assembling Diblock Copolymer Systems: Characterization of

Poly(isoprene-*b*-methyl methacrylate) Micelles in Acetonitrile Interfaces in Self-Assembling Diblock Copolymer Systems: Characterization of Poly(isoprene-*b*-methyl methacrylate) Micelles in Acetonitrile. *J. Phys. Chem. B* **1999**, *103*, 2487–2495. (b) Schillen, K.; Yekta, A.; Ni, S.; Farinha, J. P. S.; Winnik, M. A. Characterization of Polyisoprene-*b*-Poly(methyl methacrylate) Diblock Copolymer Micelles in Acetonitrile. *J. Phys. Chem. B* **1999**, *103*, 9090–9103.